RSC Advances

ROYAL SOCIETY OF CHEMISTRY

www.rsc.org/advances

Molecular Dynamics Study on Mechanism of Preformed Particle Gel Transporting through Nanopores: Surface Hydration

Heng Zhang†, Ying Ma†, Qingquan Hao‡, Hua Wang†, Gang Liu†, Shiling Yuan*†

† *School of Chemistry and Chemical Engineering, Shandong University, Jinan 250199, P. R. China*

‡ *School of Chemical Engineering, East China University of Science and Technology, Shanghai, 200237, P. R. China*

Abstract: Preformed particle gels (PPG) as a potential oil-displacement agent, composed of cross-linked partially hydrolyzed polyacrylamide, is being applied to promote the oil recovery ratio in several oil fields in China. At the molecular level, a molecular dynamics simulation on PPG transporting through nanopores was performed to investigate its propagation mechanisms during gel injection. Initially, a silica nanopore was modeled as a finite-length cylindrical pore, in which the inner surface was fully hydroxylated. Then, a swollen PPG with a smaller size was put in. After a long enough simulation, the hydration layer induced by silica pore surface was discussed to study the effect on the transport of PPG. Steered molecular dynamics was then used to mimic the transport of PPG under injection pressure. The results suggested that this hydration layer served as a physical and energy barrier that keeps PPG away from the pore surface by analyzing from radial number density distributions, orientational arrangement, dependence of the diffusive mobility, hydrogen bonding characteristics and potential of mean force. Also, the lubrication of the hydration layer may reduce the resistance that PPG has to overcome while transporting through nanopores. These factors will promote the propagation of PPG within nanopore and reduce the injection pressure. The simulated results were expected to provide the molecular level insights into the mechanism of PPG transporting through nanoporous media or the molecular design of optimized PPG.

1. Introduction

Excess water production is becoming a major problem in mature oil fields, after the oil reservoir is subject to long term water flooding process. It makes a well unproductive, leading to both an abandonment of wells and a reduction in oil production. What's more, excess water increases the costs related to corrosion,

water/oil separation etc.[1,2] Therefore, water shutoff or conformance control become a significant environmental and financial challenge for the whole petroleum industry.

Fortunately, gel treatment has been proved to be successful in conformance control for oil reservoirs. The successful gel treatment can effectively reduce channeling or fractures without influencing oil productivity. Traditionally, in situ gels are used in oil fields. Polymers and cross-linkers are injected simultaneously into a target formation and react to form gels under reservoir conditions to seal the formation. However, the in situ gels have several drawbacks, such as the lack of gelation time control, the uncertainty of gelling due to shear degradation, the chromatographic fractionation, and the dilution by formation water, etc.[3,4] Recently, preformed particle gels (PPG) have been widely studied and applied for conformance control. Their main components are cross-linked partially hydrolyzed polyacrylamide. They are formed in surface facilities before injection, and no gelation occurs in the reservoir; therefore, the gelation process is not affected by the environments of formation.[5]

The effect of gel treatments mostly depends on the ability of the gels transporting through fractures and channels. Therefore, it is important to understand how a swollen PPG in the solution behaves during its flow in the nanopore, and even how to optimize PPG design in the following experiments. Till now, extensive efforts have been made to understand the propagation of gels through fractures or high permeability sand packs, both theoretically and experimentally [6-8]. Seright and co-workers have extensively investigated the effects of fracture conductivity or tube diameter and gel injection rate on in situ extrusion behavior through open fractures and tubes.[9,10] Bai *et al.* [11,12] performed many experiments to investigate the propagation of PPG through porous media (for example, six transport patterns were identified, including “direct pass”, “shrink and pass”, “trap”, etc) and the influencing parameters such as particle size, swelling capacity, injectivity and etc. Numerical simulations were also done by Wang *et al.* [13] to obtain the influences of injection rate, suspension concentration, mean particle diameter, etc., and the verification is proved by the experimental data.

These experimental investigations help us to understand the mechanism of PPG transporting through porous media. However important details of transporting process are still difficult to obtain by experimental technologies at the molecular level. Moreover, experiments using fractures to obtain the gel rheological properties are both expensive (for core materials and casting) and time-consuming.[5] To gain more microscopic insights into the transport process, computational simulations which are considered as important supplements to experimental observations were carried out. However, to our best knowledge, simulation studies about the propagation of PPG transporting through nanopores are really scarce.

In this work, we carried out a series of simulation studies of the "direct pass" transport mechanism (i.e. one of the transport pattern in Bai's experiment [11]) of PPG within silica nanopores using molecular dynamics methods. Silica was selected as it is a major composition of glass micromodels or rock minerals (e.g. quartz sandstone) in many geological environments. Steered molecular dynamics was used to mimic the transport of PPG under injection pressure. During the transport process, our attentions were mostly focused on the effect of ordered water induced by silanol groups near the surface of nanopore, which was believed that can reduce the injection pressure. Some observations from the simulation may be useful in understanding the transport mechanism or optimizing PPG design.

2. Simulation Method

2.1 Modeling of Silica Nanopore and PPG

A silica nanopore was modeled in the same manner as described in previous publications [14, 15], i.e., as a finite-length cylindrical nanopore normal to the surface of a film of α-quartz crystal. The procedure can be divided in two stages. First, a cylindrical hole of diameter d = ~5 nm was carved in an α-quartz block with the dimensions $L_x = L_y = 8.35$ nm and $L_z = 27.4$ nm, by removing all the atoms lying along z axis within the diameter. In this model, the diameter of the cylindrical pore was set just a bit bigger than that of the swollen PPG. The length of nanopore was set to be long enough, which was sufficient to satisfy the minimum image convention and provide space for pulling simulations to take place along z axis. Then the pore

surfaces were fully hydroxylated with silanol groups to saturate the bare Si atoms on the internal silica nanopore, resulting into two types of silanol groups, i.e., Si-$(OH)_2$ (germinal silanols, denoted as Q^2) and Si-OH groups (isolated silanols, denoted as Q^3)[16]. (Figure 1a and S1). The density of silanol groups is about 8.0 –OH per nm^2, which is in accordance with ref [17-19]. However, one must keep in mind that in practice the in-situ EOR is normally carried out under complex underground conditions using solutions containing polymers and/or surfactants. The surface chemistry and pH conditions of the silica nanopores were not easy to determine. Here we adopt a simplified model which may not accurately reflect the exact surface chemistry and solution environment. However many experiment and simulation studies suggest that minor differences have limited impact. Following discussions were based on this simplified model.

Four cross-linked HPAM (-$[CH_2CHCONH_2]_{3a}$-$[CH_2CHCOO^-]_a$-, partially hydrolyzed polyacrylamide,) fragment with DP=100 and DH=25% (DP, degree of polymerization, DH, degree of hydrolysis) were constructed with cross linker -$COO(CH_2)_2NCH_3CH_2$-. After a short equilibrium in vacuum, the structure of preformed particle gel was derived (Figure 1b).

To study the mechanism of PPG transporting through silica nanopores, the derived PPG was settled in the cylindrical nanopore as depicted in figure 1c. After water molecules added in the silica pore, a series of MD and SMD simulations were then performed.

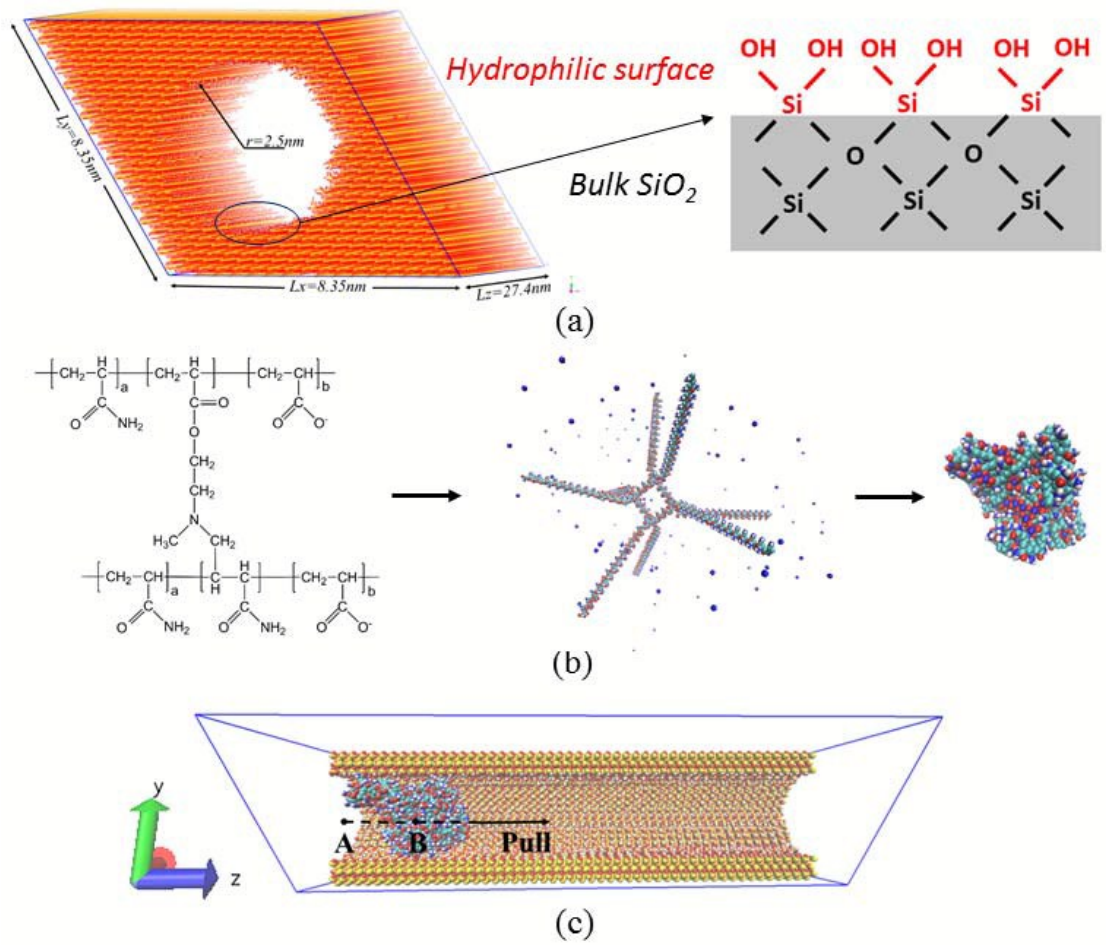

Figure 1. The models and flowchart of molecular simulation.

(a) A silica nanopore with a diameter of 5 nm and length of 27 nm which is made up of bulk SiO_2 and hydrophilic surface. The pore surface was functionalized with OH groups. The bulk SiO_2 was constrained during all simulations. (b) Scheme of preformed particle gel. Four partially hydrolyzed polyacrylamide chains were linked and then run to be equilibrium in vacuum to get the PPG. (c) Schematic illustration of the initial structure and pulling direction in steered molecular dynamics simulation.

Table 1 Force field parameters for PPG and SiO_2 used in this work*

atom	σ(nm)	ε(kJ/mol)	q(e)
CH_3	0.379	0.753	0
CH_2	0.395	0.586	0
CH	0.423	0.544	0
$C(CONH_2)$	0.336	0.406	0.38
$O(CONH_2)$	0.263	1.725	-0.38
$N(CONH_2)$	0.298	0.877	-0.48
$H(CONH_2)$	0	0	0.24
$C(COO^-)$	0.336	0.406	0.27
$O(COO^-)$	0.263	1.725	-0.635
Si	0.339	2.447	0.310
H(Si-OH)	0	0	0.400
O(Si-OH)	0.295	0.850	-0.710

*The parameters were derived from GROMOS 43a2 united-atom force field [20] and ref [21], [22] for PPG, ref [23] for silica nanopore. Charges of atoms of bulk SiO_2 are set to zero. Other atoms' force field parameters were not shown for clarity.

2.2 Simulation Details

Molecular dynamics simulations were performed using the GROMACS software package (version 4.5.4). [24] The Gromos 43a2 force field [20] was adopted for all of the potential function terms to calculate the interatomic interactions. The total potential energy was given as a combination of valence terms, including bond stretching, angle bending, torsion and nonbonded interactions. The nonbonded interactions between atoms were described by the Lennard-Jones potential, and the standard geometric mean combination rules were used for the van der Waals interactions between different atom species. The simple point charge (SPC) model [25] was used to describe water molecules. The nonbond parameters of SiO_2 were also taken from Gromos 43a2 force field to be consistent with PPG. The charge distribution of the surface atoms were taken from Hoffmann and Berendsen's work [23] which gave a good prediction of adsorbed water layers on the silicon oxide surface. Our previous work referencing this force field has also derived reasonable results [26, 27]. Actually, there is a more accurate force field for silica to choose. Heinz's group [17, 18] has developed a force field for silica that overcomes many prior limitations, and included surface ionization. The force field is fully consistent with the chemical properties of silica at the atomic and interfacial scale. A comprehensive surface model database was also introduced that provides realistic surface models for any silica surface chemistry and pH for variable ionization.

Each of the systems was initialized by minimizing the energies of the initial configurations using steepest descent method. Following the minimization, a 40 ns MD simulation under canonical ensemble (NVT) was carried out for each system, with a time step of 2 fs. During the minimization and the equilibration MD simulation, position restraints were applied to the silica block except the hydrophilic surface (Figure 1a). In all simulations, the temperature was kept constant at 298 K by the

v-rescale thermostat algorithm [28]. Bond lengths were constrained using the LINCS algorithm [29] and periodic boundary conditions were applied in all directions. Short-range nonbonded interactions were cut off at 1.2 nm, with long-range electrostatics calculated using the particle mesh Ewald method. [30] Trajectories were stored every 10 ps and visualized using VMD 1.9.2. [31] The last 5 ns trajectories were used for further analysis.

In order to simulate the driven conditions from the water flooding, biased MD simulations, named steered molecular dynamics (SMD)[32] or pulling simulations were conducted using the pull code of the GROMACS package. Structures from the end of equilibrated MD trajectories were used as starting configurations for pulling simulations. The driving force was performed on the whole PPG (i.e., pulling group). A point on the central axis of the nanopore was selected as an immobile reference for the pulling simulations. The distance between the selected point and the center of mass (COM) of PPG was about 2 nm. Figure 1c shows a schematic representation of the force on the pulling group. For each system, the pulling group was pulled away from its original position along the z-axis over 1.5 ns, using a spring constant of 1000 $kJ \cdot mol^{-1} \cdot nm^{-2}$ and a pull rate of 0.01 $nm \cdot ps^{-1}$. The pull rate was set very slow to make sure the pulling did not deform the elements of systems. The other calculation details used the same methodology of the equilibrated MD simulations.

3. Results and Discussion

3.1 Swelling of PPG

After a 40ns MD simulation, the system reached equilibrium from the view of RMSD and the SASA (solvent access surface area) of PPG in figure 2, which kept constant with only a small fluctuation after 18 ns. From the SASA, one can also speculate that the PPG particle went through a swelling process in the nanopore. A similar process were also observed in our previous work [33], which was deduced as results from the strong hydration of hydrophilic groups of PPG ($-COO^-$ and $-CONH_2$). The expansion ratio of PPG after swelling was about 1.27, calculated as $SASA_{after}/SASA_{before}$. In the simulation, the expansion of PPG in the solution is

consistent with experiments qualitatively, and the expansion ratio derived here is much smaller than the experimental observation quantitatively. As the molecular weight of PPG simulated here is quite small comparing with that in the experiment.

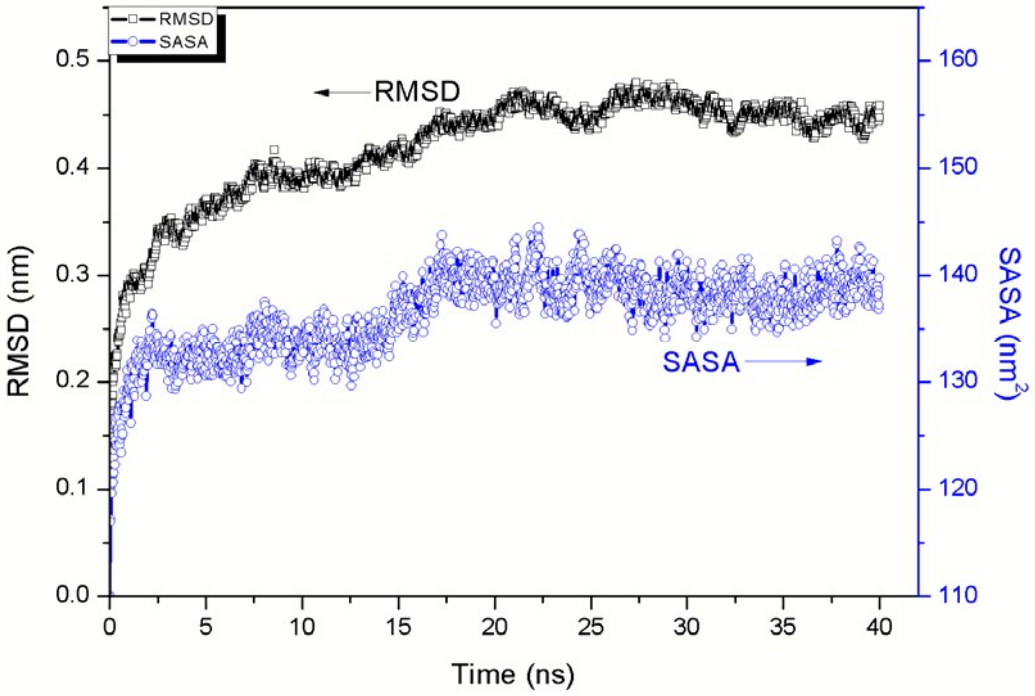

Figure 2. RMSD and solvent access surface area (SASA) of PPG versus time during 40ns MD simulation.

3.2 Structure properties within silica nanopore

The structural properties of PPG and water inside the nanopore were investigated to explore their distribution. The radial distribution of oxygen atoms of water and carbon atoms of PPG were computed from the pore center to the inner surface as illustrated in figure 3a. The peaks of oxygen and hydrogen atoms of silanol groups at about 2.5 nm represent the radius of the pore. The swollen PPG mostly located in the middle of the pore as the density profile decreased with the radial position. One evident peak of oxygen atoms of water near silica surface was found which corresponds to the hydration layer. The densely packed hydration layer that induced by silanol groups has a thickness of about 0.4nm.

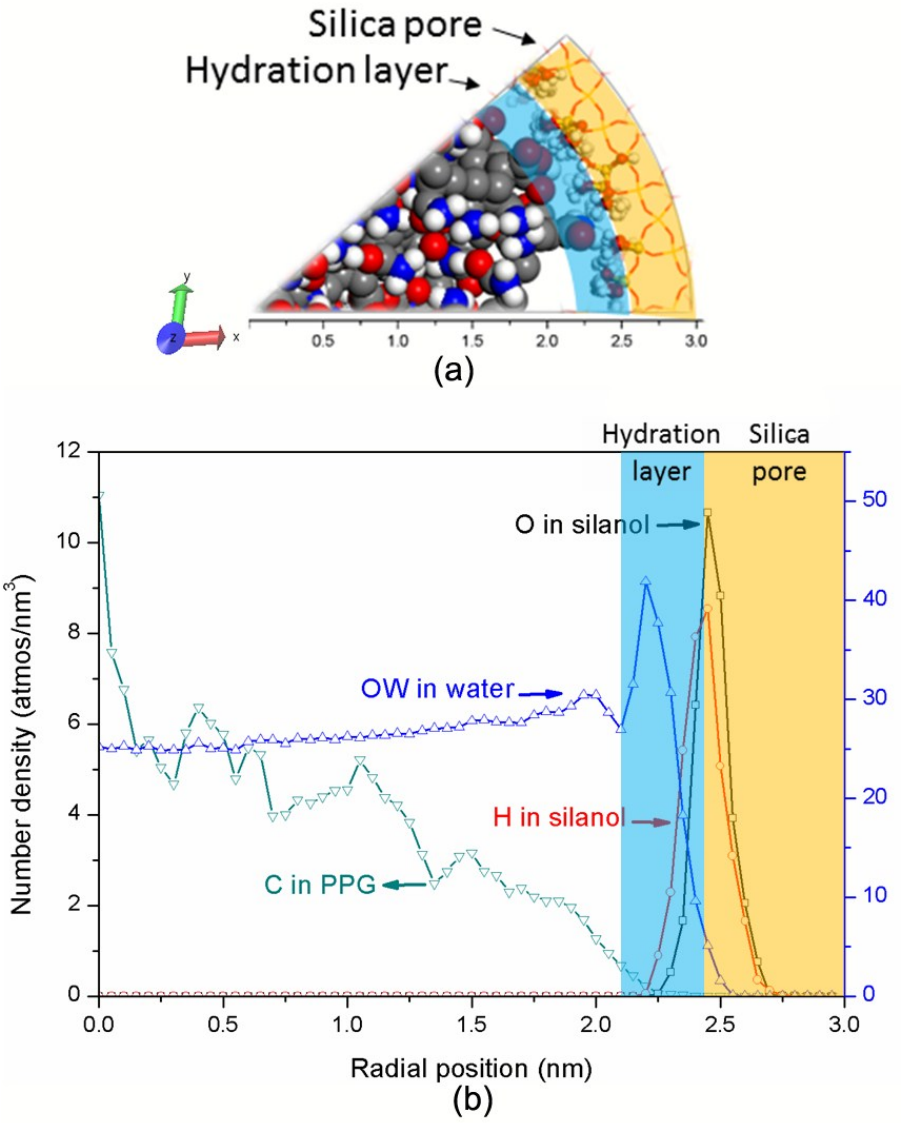

Figure 3. Radial density profiles of atoms inside the silica nanopore.
(a) Illustration of the calculation of radial density profiles from the cylindrical axial view. PPG was depicted in CPK model, surface hydrophilic groups of nanopore was displayed in ball and stick model, and the bulk SiO_2 in line model. Atom color scheme: O, red; Si, yellow; C, gray; N, blue; H, white. (b) Number density profiles with respect to the central axis of the pore along the cylindrical radial direction. The silica pore was colored yellow, and the hydration layer was colored blue.

Preferential orientation of water molecules in hydration layer is very important to evaluate the hydration strength of silica pore surface. The angle θ was defined as the angle between dipole direction of water molecule and the vector passing through the oxygen atom of water molecule, pointing to center, as illustrated in figure 4(a). The orientation of water molecule in hydration layer was highly ordered as concluded from figure 4(b). The value of cos (θ) mostly concentrated on around ±0.8, which

indicates that most of water dipoles in hydration layer pointed to the axis of the cylinder pore. This is mainly due to the geometry of hydrogen bonds formed between surface water and the silanol groups. The oxygen atoms of surface water prefer to serve as acceptors to form hydrogen bonds with hydrogen atoms of silanol groups which served as donors.

From the structural properties analyzed above, a densely packed and highly ordered hydration layer was observed with a thickness of 0.4nm. It was believed to have vital effect on the transport of PPG in the pore. In the following of the paper, attentions were focused on the properties and effect of this hydration layer.

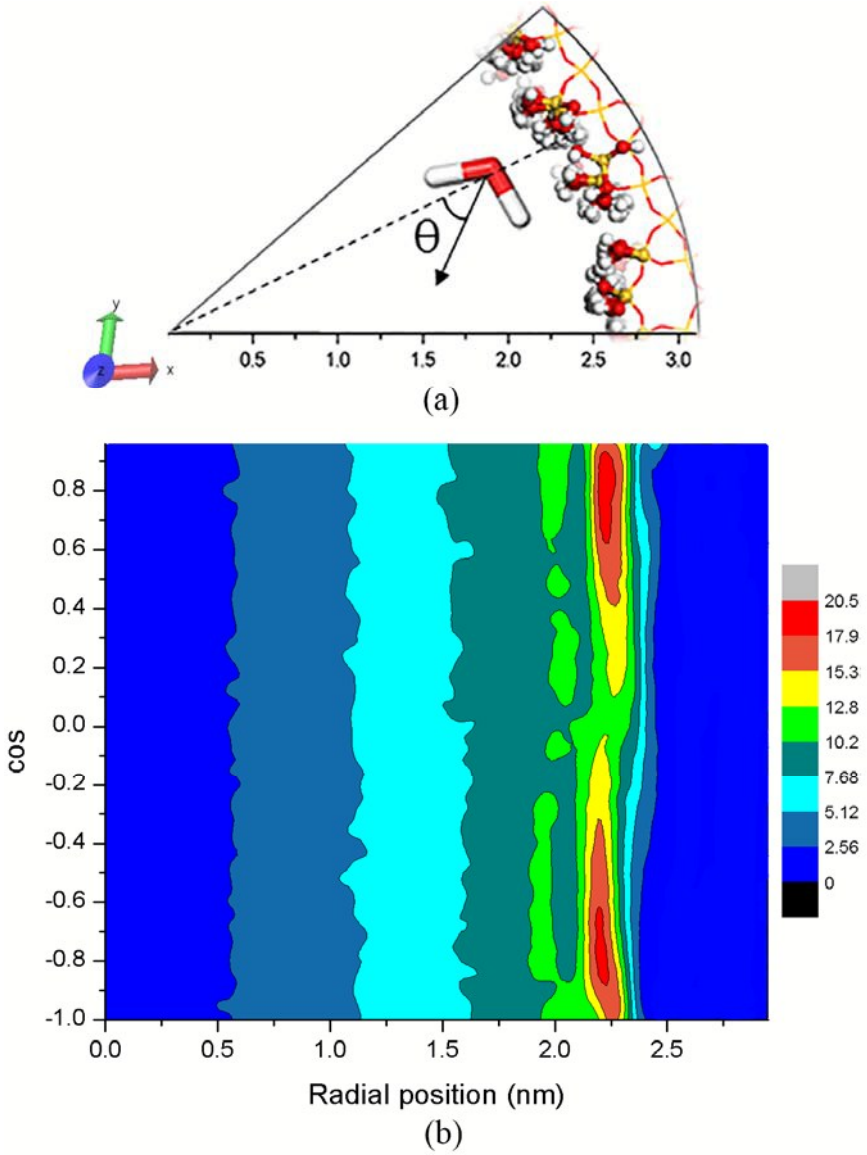

Figure 4. Distribution of the orientation of hydration layer water in the silica nanopore. (a) θ is defined as the angle between solvent molecule's dipole vector and the vector pointing from the pore surface to center. (b) Distribution of cos (θ).

3.3 Dynamic properties of water confined in silica nanopore

Figure 5 visualized how the solvent diffusion coefficients inside the nanopore depend on the radial position. The diffusion coefficients of water molecules are based on their mean square displacements paralleling to the pore axis [34, 35]. For calculating anisotropic diffusion coefficients near the pore surface, bulk diffusion coefficients were also included as dashed horizontal lines for comparison. Figure 5 shows that solvent mobility near the pore surface was significantly reduced compared with the bulk phase (about $4.14 \times 10^{-5} cm^2/s$). Toward the silica surface, the solvent mobility decreases drastically and even approaches to zero (R > 2.0 nm), reflecting that water molecules nearly immobilized by hydrogen bonding to surface silanol groups. We name water molecules in the first hydration layer as the bound water. This tightly bounded hydration layer could serve as a natural physical barrier to keep PPG from interacting with the nanopore directly.

While beyond this region, water's diffusion coefficient increased slowly to bulk value. The region between the first hydration layer and bulk phase (1.2 nm < R <2.1 nm) were called the second hydration layer which consist of trapped water. It is quite different from the first hydration layer near the silica pore surface which was made up by bounded water molecules. This region can also be recognized from figure 3 and 4. The second hydration layer's mobility were only slightly impacted by forming hydrogen bonds with the first hydration layer water as illustrated in figure 5.

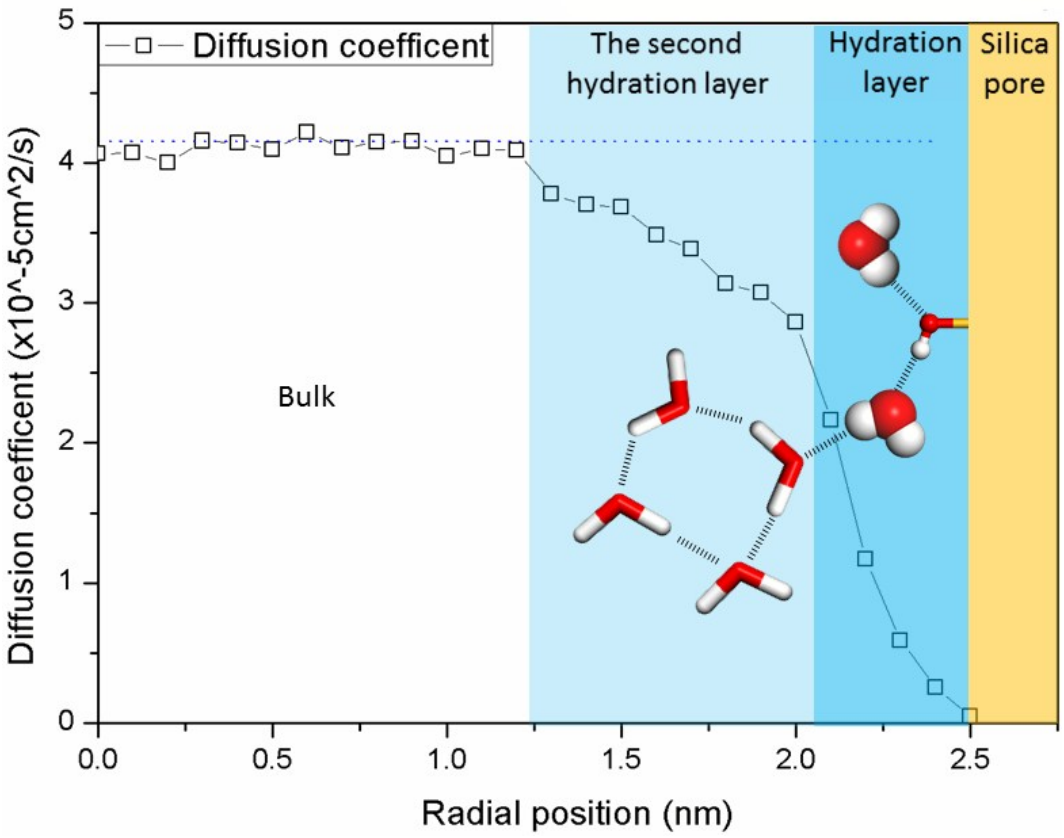

Figure 5. Diffusion coefficients paralleling to the pore axis of water in different radial positions. Dashed line indicate the bulk value. The silica pore was colored yellow; the first hydration layer colored blue; the second hydration layer colored light blue. The silanol groups at silica pore surface were represented with ball and stick model; the bound water molecules within the first hydration layer displayed with CPK model; the trapped water molecules within the second hydration layer represented with stick model. The hydrogen bonds between them were illustrated as hash lines.

3.4 Hydrogen bonds properties

The dynamics of interfacial water molecules and their structural organization are correlated with the network of hydrogen bonds formed between these water molecules and the pore surface. Coordination of the solvent molecules was then analyzed from the radial distribution of their hydrogen bonds. Generally, either a geometric or an energetic criterion is used to define a hydrogen bond. In this work, we employed a purely geometric hydrogen bonding criteria, i.e. the distance between donor and acceptor less than 0.35nm, and the angle Acceptor…Donor-Hydrogen less than 30 degree [36,37]. Figure 6 illustrated hydrogen bonds between water molecules and surface silanol groups, those among water molecules, and those between water and

PPG. In the silica nanopore, water molecules are hydrogen bonded throughout the pore, either with PPG, silica pore surface or other water molecules. The hydrogen bonds formed between water and PPG distributes uniformly, except in the central area where more donors and acceptors belonging to the PPG distributed. Around the surface region (2.0 nm < R < 2.5 nm), water molecules prefer to forming hydrogen bonds with silanol groups, with the biggest 2.5 water-silanol hydrogen bonds per water molecule. While beyond the surface region, water-water hydrogen bonds is preferred, with an average of 1.9 hydrogen bonds per molecule. The coordination for water-water hydrogen bonds approaches bulk value just beyond the immediate surface region and then keeps constant toward the pore center.

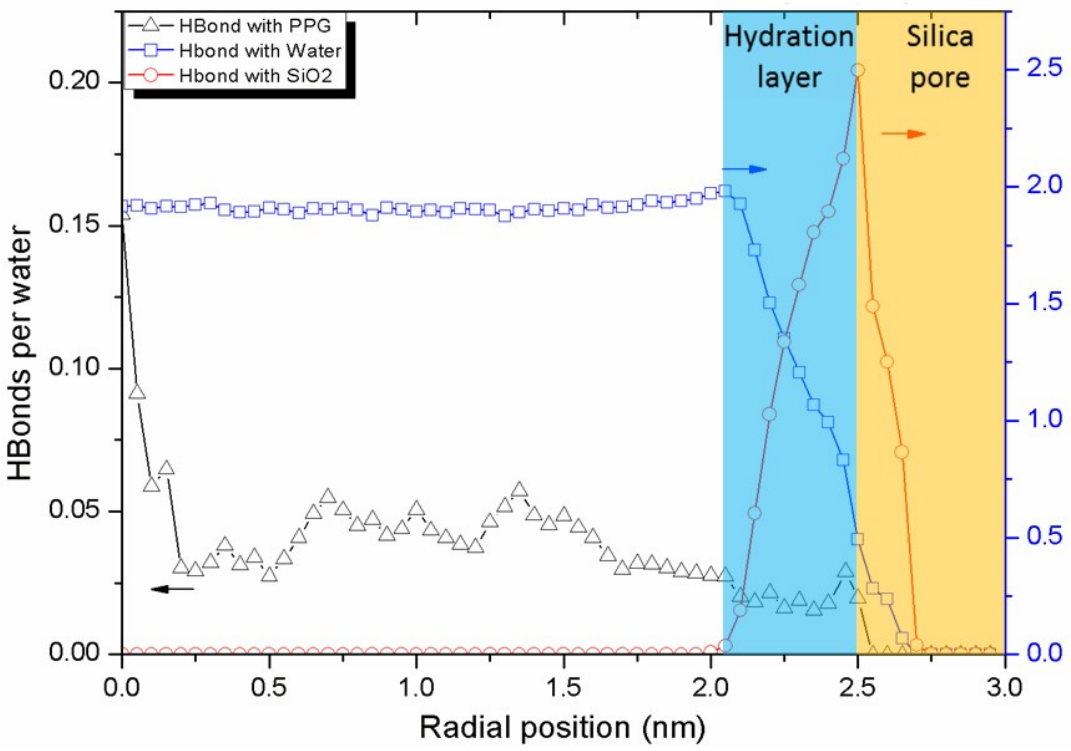

Figure 6. Radial projection of the hydrogen bond network of water in the silica nanopore.

The dynamics of hydrogen bonds formed between PPG and the pore surface, as well as that between water and surface, can reflect the strong or weak interaction between PPG or water and nanopore surface. Figure 7 illustrated the time correlation function $C_{HB}(t)$ for hydrogen bond formed between SiO_2 and PPG or water molecules. $C_{HB}(t)$ is defined as:

$$C_{HB}(t) = \frac{\langle h(0)h(t)\rangle}{\langle h(0)\rangle} \quad (1)$$

where the variable *h(t)* is unity when a particular pair of atoms is hydrogen bonded at time *t* according to the definition, otherwise *h(t)*=0. The angular brackets denote an ensemble average over all hydrogen bond pairs investigated. The correlation function of hydrogen bond between PPG and nanopore surface decays rapidly compared with that between water and nanopore surface. The quantified hydrogen bond lifetime, obtained by fitting the corresponding correlation functions with exponential function, suggests that water molecules in hydration layer interact with the pore surface more tightly than PPG. The hydrogen bond network between silica nanopre surface and water molecules seems more stable.

Around the surface region (2.0 nm<R<2.5 nm), hydrogen bonding characteristics (Figure 6, 7) is in agreement with the radial number density distributions (Figure 3), orientational arrangement (Figure 4), and the dependence of the diffusive mobility (Figure 5).

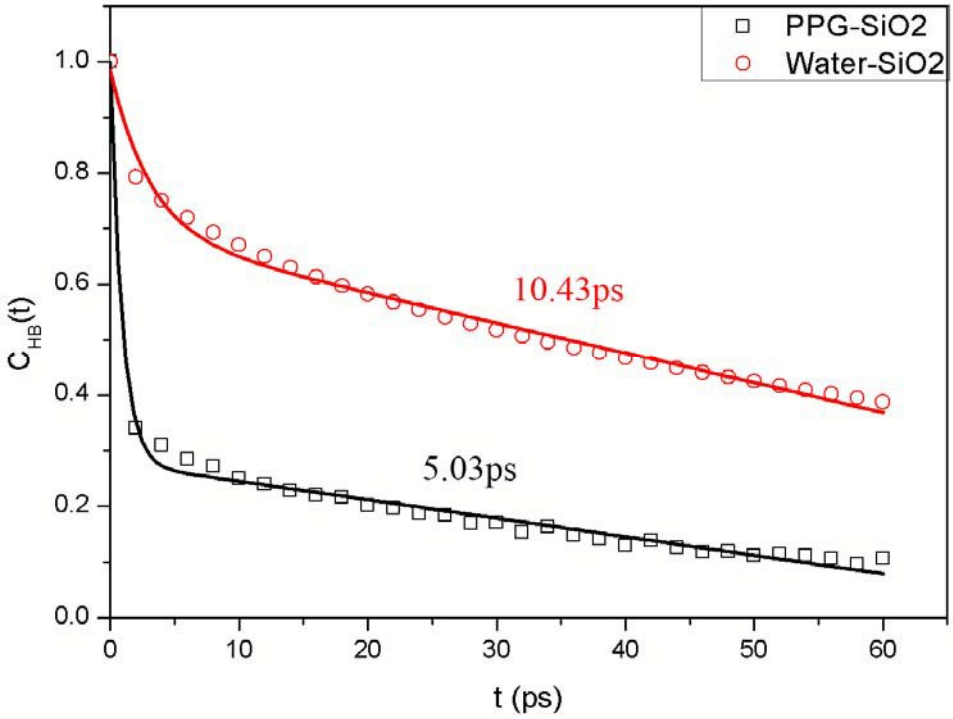

Figure 7. Time correlation function $C_{HB}(t)$ for hydrogen bond formed between SiO_2 and PPG or Water.

3.5 Interactions between silica nanopore and water

From the discussion above, we notice that the hydrophilic surface of silica nanopore induced a typically strong hydration layer around it via non-bond interactions, such as van der Walls, electronic or hydrogen bonds. The first obligation step for PPG to interact with the pore surface directly is to overcome the physical and energy barrier arise from this hydration layer. The energy barrier is highly associated with the physical chemistry properties and structure of the nanopore surface.

The interaction between silica nanopore and water molecules can be reflected from the potential of mean force (PMF). The PMF was calculated by the radial distribution function g(r) of the silica nanopore and water through the equation $E_{(r)} = -k_B T \ln g(r)$, where k_B is Boltzmann's constant and T is the simulation temperature. The energy profiles were illustrated in figure 8, from which the following conclusions can be made. i) The contact minimum (CM) in energy profile is at about 2.2 nm, corresponding to the direct contact between water and silica nanopore surface. ii) The second minimum is at a radial position of 1.95 nm, which corresponds to the solvent-separated minimum (SSM). Both CM and SSM determine the binding affinity of water to the silica nanopore surface. iii) The CM and SSM are separated by a desolvation barrier (BARR) that must be overcome for transitions between the two minima. The calculated PMF tend to be zero with the increasing distance between the silica nanopore surface and water.

The binding energy barrier for the silica nanopore and water is related to SSM and BARR, i.e., $\triangle E^{+}=E_{BS}-E_{SSM}=0.3$ kJ/mol, while the dissociation energy barrier for silica nanopore and water is related to CM and BARR, i.e., $\triangle E^{-}=E_{BS}-E_{CM}=1.09$ kJ/mol. For interacting with the silica surface, the energy barrier PPG has to overcome is related to $\triangle E^{-}$. Form the energy point of view (figure 8), it's quite easy for silica nanopore surface to form a hydration layer, and difficult to dissociate it, which means the hydration layer is energetically stable.

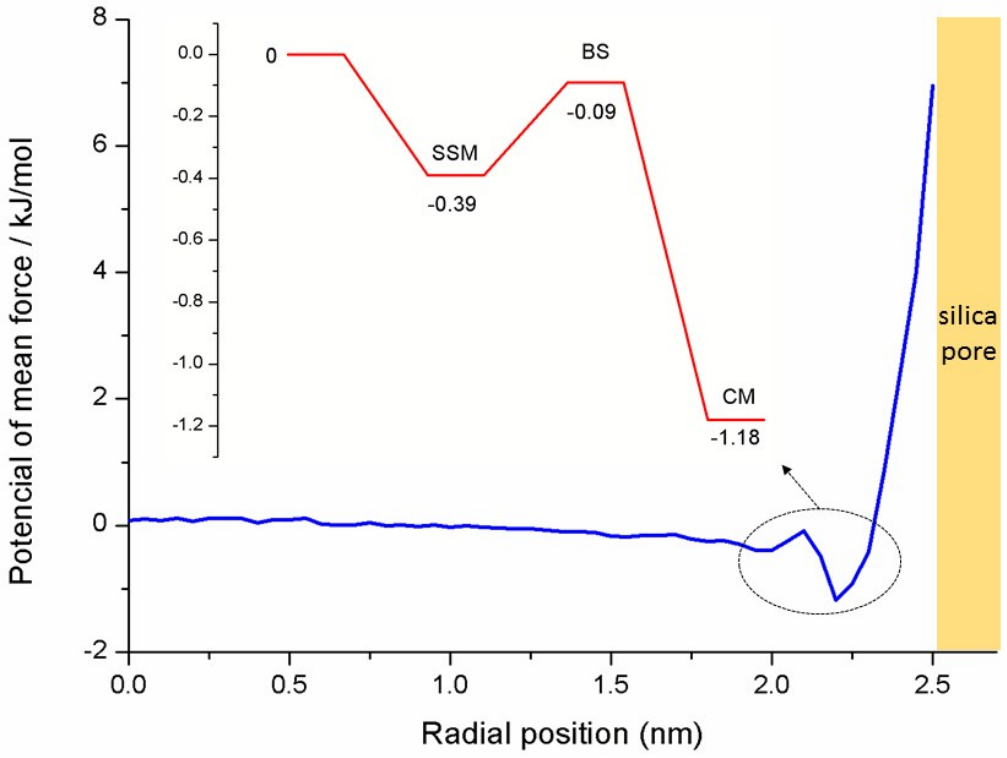

Figure 8. Potential of mean force between water and silica nano pore.

Those properties analyzed above suggested that the silica nanopore can induce a densely packed, highly ordered, and tightly bounded energetically stable hydration layer, with intermolecular interactions between water and silica nanopore surface. For PPG, it has to break the stable hydrogen bond networks around the surface region. These water molecules that tightly bounded to the surface served as a physical and energy barrier, which keeps PPG from directly interacting with the pore surface.

3.6 Process of the PPG transport through nanopore

External forces were then exerted on the COM of PPG to simulate the driven forces of water flooding during the process of oil recovery. Figure 9 illustrated the forces and distance as a function of pulling time. Within the 5.0 nm nanopore, the pull process can be approximately divided into three stages, according to the variation of the force and COM distance. During the first 0.4ns, stage I, the force increases rapidly while the COM of PPG moves slowly. To move the PPG forward along the nanopore, the external force has to overcome the resistance related to PPG, which includes the interaction between PPG and silica surface, the broken of hydrogen bonds networks

near PPG, etc. As the force increased to 3.5×10^3kJ/(mol·nm), PPG starts to move slowly along the nanopore (stage II). After a series of adjustment of external forces during stage II, the resistance and pulling force come to equilibrium. At the breaking point of stage III (1.1 ns), the pull force reaches maximum and keeps relatively constant subsequently.

This three stages model illustrates that at the initial of PPG's movement within nanopore, external forces should be added to overcome the resistance arise from the broken of hydrogen bond network around PPG, and interactions between PPG and silica surface. Fortunately the silanol group induced hydration layer around nanopore surface screened that interaction between PPG and pore. Once in the II and III stage, the lubrication of this hydration layer may also reduce the resistance that PPG has to overcome while moving through the nanopore, as the maximum force exerted on PPG was larger for the system without hydration layer (figure S2). These will promote the propagation of PPG within nanopore and reduce the injection pressure during gel treatment.

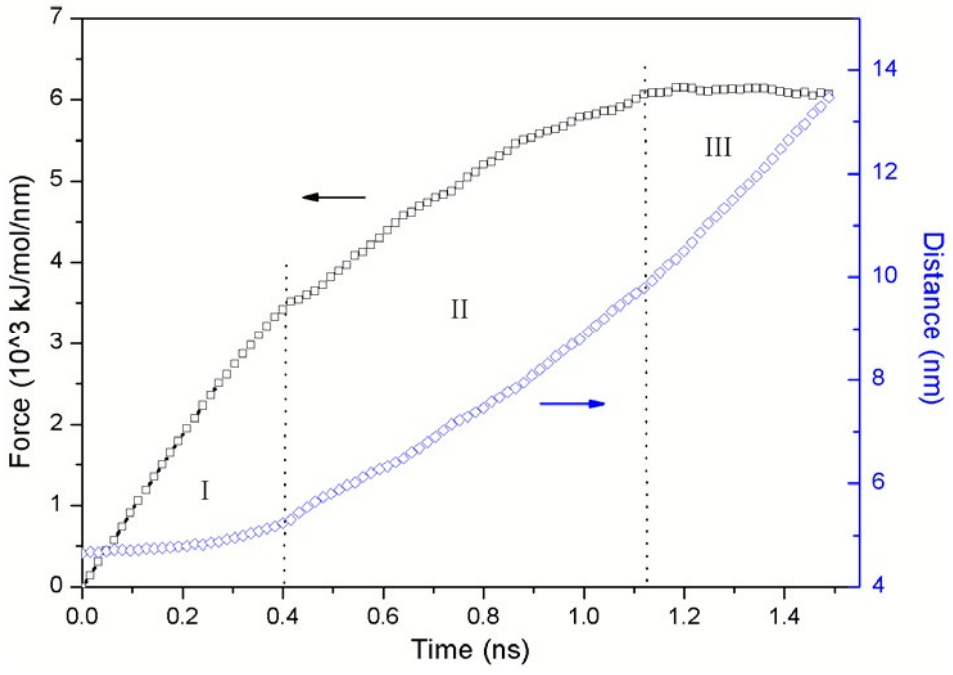

Figure 9. Profile of the external force extend on the PPG during steered molecular dynamics.

4. Conclusion

In this paper, MD simulations were conducted to investigate the mechanism of

PPG transporting through silica nanopores. Swelling of PPG was observed by measuring the SASA, which coincides with the previous study. The structural features inside the nanopore suggested that a densely packed and highly ordered hydration layer was formed around the surface region (2.0<R<2.5nm). The water molecules in hydration layer interact with the nanopore surface via non-bond interactions, such as van der Walls, electronic and hydrogen bonds, and their diffusion coefficient along the pore axis was highly reduced. The interaction between nanopore and water molecules suggests that this layer is energetically stable. This hydration layer constrained by the silica nanopore surface was believed to have vital effect on the transport of PPG within nanopore.

Steered molecular dynamics simulations were then performed to study the transport process of PPG. External forces were exerted on PPG to mimic the driven force of water flooding in EOR. Detailed information about the process was achieved. Briefly, three stages were distinguished during the pull simulation. Resistance has to be overcome before PPG can move along the pore, which mainly results from the interaction between PPG and silica pore, and the broken of hydrogen bond networks near PPG (stage I). After adjustments in stage II, external force and resistance finally came to equilibrium (stage III), resulting into the movement of PPG in the nanopore.

Figure 10 provide a molecular level insight into the effect of hydration layer during PPG transport through silica nanopores in enhanced oil recovery. It served as a physical and energy barrier that keeps PPG away from the pore surface, and screened the interaction between PPG and pore. This largely reduced the resistance that PPG has to overcome during transport. During PPG's transport the lubrication of the hydration layer can also help. All of these will promote the propagation of PPG within nanopore and reduce the injection pressure.

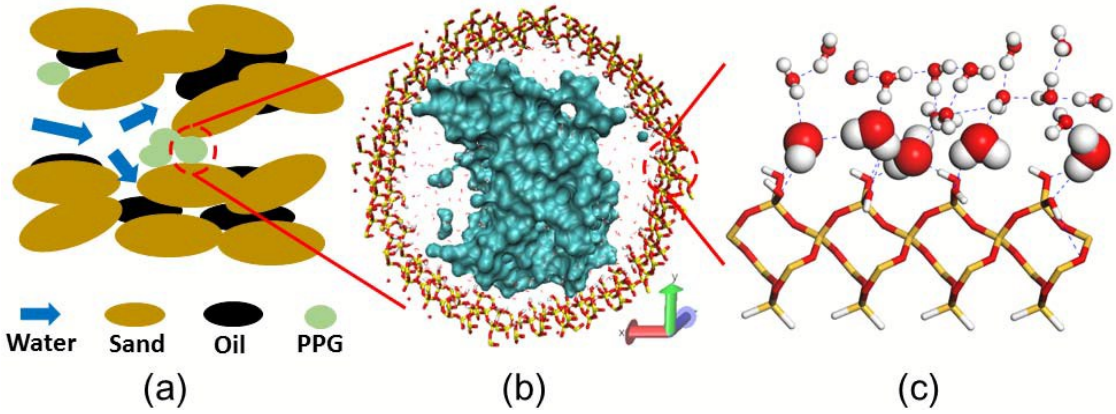

Figure 10. Schematic illustration for the effect of hydration layer during PPG transporting through silica nanopores from a stepwise zoomed in perspective.

(a) Injection of PPG for profile control; (b) PPG passing through a nanopore, represented with its solvent access surface (c) hydration layer induced by silanol groups in pore surface which keep PPG from directly interacting with silica nanopore, and lubricate during its propagation. Water molecules within the first hydration layer were represented with CPK model, while in the second hydration layer were displayed in ball and stick model. Hydrogen bond network between them was illustrated as blue dashed lines.

Acknowledgement

We gratefully appreciate the financial support from the National Science Foundation of China (No. 21573130)

References

1. Seright, R. In *Washout of Cr (III)-Acetate-HPAM Gels from Fractures*, International Symposium on Oilfield Chemistry, **2003**; Society of Petroleum Engineers.

2. Elsharafi, M. O.; Bai, B. Effect of Weak Preformed Particle Gel on Unswept Oil Zones/Areas during Conformance Control Treatments. *Industrial & Engineering Chemistry Research* **2012,** *51* (35), 11547-11554.

3. Bai, B.; Li, L.; Liu, Y.; Wang, Z.; Liu, H. In *Preformed particle gel for conformance control: factors affecting its properties and applications*, SPE/DOE Symposium on Improved Oil Recovery, **2004**; Society of Petroleum Engineers.

4. Chauveteau, G.; Tabary, R.; Le Bon, C.; Renard, M.; Feng, Y.; Omari, A. In *In-depth permeability control by adsorption of soft size-controlled microgels*, SPE European Formation Damage Conference, **2003**; Society of Petroleum Engineers.

5. Zhang, H.; Challa, R. S.; Bai, B.; Tang, X.; Wang, J. Using screening test results to

predict the effective viscosity of swollen superabsorbent polymer particles extrusion through an open fracture. *Industrial & Engineering Chemistry Research* **2010,** *49* (23), 12284-12293.

6. Moghadam, A. M.; Sefti, M. V.; Salehi, M. B.; Koohi, A. D. Preformed particle gel: evaluation and optimization of salinity and pH on equilibrium swelling ratio. *Journal of Petroleum Exploration and Production Technology* **2012,** *2* (2), 85-91.

7. Zhao, G.; Dai, C.; Zhao, M. Investigation of the Profile Control Mechanisms of Dispersed Particle Gel. *PLoS One*. **2014**, *9*(6), e100471.

8. Feng, Q.; Chen, X.; Zhang, G. Experimental and Numerical Study of Gel Particles Movement and Deposition in Porous Media After Polymer Flooding. *Transport in Porous Media* **2013,** *97* (1), 67-85.

9. Seright, R. S. Gel propagation through fractures. *SPE Production & Facilities* **2001,** *16* (04), 225-231.

10. Seright, R.; Lee, R. In *Gel treatments for reducing channeling in naturally fractured reservoirs*, SPE Permian Basin Oil and Gas Recovery Conference, **1998**; Society of Petroleum Engineers.

11. Bai, B.; Liu, Y.; Coste, J.-P.; Li, L. In *Preformed particle gel for conformance control: transport mechanism through porous media*, SPE/DOE Symposium on Improved Oil Recovery, **2004**; Society of Petroleum Engineers.

12. Goudarzi, A.; Zhang, H.; Varavei, A.; Taksaudom, P.; Hu, Y.; Delshad, M.; Bai, B.; Sepehrnoori, K. A laboratory and simulation study of preformed particle gels for water conformance control. *Fuel* **2015,** *140*, 502-513.

13. Wang, J.; Liu, H.; Wang, Z.; Xu, J.; Yuan, D. Numerical simulation of preformed particle gel flooding for enhancing oil recovery. *Journal of Petroleum Science and Engineering* **2013,** *112*, 248-257.

14. Elola, M. D.; Rodriguez, J.; Laria, D. Structure and dynamics of liquid methanol confined within functionalized silica nanopores. *The Journal of Chemical Physics* **2010,** *133* (15), 154707.

15. Elola, M. D.; Rodriguez, J.; Laria, D. Liquid Methanol Confined within Functionalized Silica Nanopores. 2. Solvation Dynamics of Coumarin 153. *The Journal of Physical Chemistry B* **2011,** *115* (44), 12859-12867.

16. Zhuravlev, L. The surface chemistry of amorphous silica. Zhuravlev model. *Colloids and Surfaces A: Physicochemical and Engineering Aspects* **2000,** *173* (1), 1-38.

17. Emami, F. S.; Puddu, V.; Berry, R. J.; Varshney, V.; Patwardhan, S. V.; Perry, C. C.; Heinz, H. Force Field and a Surface Model Database for Silica to Simulate Interfacial Properties in Atomic Resolution. *Chemistry of Materials* **2014,** *26* (8), 2647-2658.

18. Emami, F. S.; Puddu, V.; Berry, R. J.; Varshney, V.; Patwardhan, S. V.; Perry, C. C.; Heinz, H. Prediction of Specific Biomolecule Adsorption on Silica Surfaces as a Function of pH and Particle Size. *Chemistry of Materials* **2014,** *26* (19), 5725-5734.

19. Ghoufi, A.; Hureau, I.; Morineau, D.; Renou, R.; Szymczyk, A. Confinement of tert-Butanol Nanoclusters in Hydrophilic and Hydrophobic Silica Nanopores. *The Journal of Physical Chemistry C* **2013,** *117* (29), 15203-15212.

20. Schuler, L. D.; Daura, X.; Van Gunsteren, W. F. An improved GROMOS96 force field for aliphatic hydrocarbons in the condensed phase. *Journal of Computational Chemistry* **2001,** *22* (11), 1205-1218.

21. Oldiges, C.; Tönsing, T. Molecular dynamic simulation of structural, mobility effects between dilute aqueous CH 3 CN solution and crosslinked PAA Part 1. Structure. *Physical Chemistry Chemical Physics* **2002,** *4* (9), 1628-1636.

22. Sulatha, M. S.; Natarajan, U. Origin of the difference in structural behavior of poly (acrylic acid) and poly (methacrylic acid) in aqueous solution discerned by explicit-solvent explicit-ion MD simulations. *Industrial & Engineering Chemistry Research* **2011,** *50* (21), 11785-11796.

23. Wensink, E.; Hoffmann, A.; Apol, M.; Berendsen, H. Properties of adsorbed water layers and the effect of adsorbed layers on interparticle forces by liquid bridging. *Langmuir* **2000,** *16* (19), 7392-7400.

24. Spoel, D.; Lindahl, E.; Hess, B.; Buuren, A.; Apol, E.; Meulenhoff, P.; Tieleman, D.; Sijbers, A.; Feenstra, K.; Drunen, R. GROMACS User Manual, version 4.5. 4; **2010**.

25. Berendsen, H.; Postma, J.; Van Gunsteren, W.; Hermans, J. Intermolecular Forces, ed Pullman B. D Reidel Publishing Company, Dordrecht, The Netherlands, **1981**.

26. Liu, Q.; Yuan, S.; Yan, H.; Zhao, X. Mechanism of oil detachment from a silica surface in aqueous surfactant solutions: molecular dynamics simulations. *The Journal of Physical*

Chemistry B **2012,** *116* (9), 2867-2875.

27. Zhang, P.; Xu, Z.; Liu, Q.; Yuan, S. Mechanism of oil detachment from hybrid hydrophobic and hydrophilic surface in aqueous solution. *The Journal of chemical physics* **2014,** *140* (16), 164702.

28. Bussi, G.; Donadio, D.; Parrinello, M. Canonical sampling through velocity rescaling. *The Journal of Chemical Physics* **2007,** *126* (1), 014101.

29. Hess, B.; Bekker, H.; Berendsen, H. J.; Fraaije, J. G. LINCS: a linear constraint solver for molecular simulations. *Journal of Computational Chemistry* **1997,** *18* (12), 1463-1472.

30. Essmann, U.; Perera, L.; Berkowitz, M. L.; Darden, T.; Lee, H.; Pedersen, L. G. A smooth particle mesh Ewald method. *The Journal of Chemical Physics* **1995,** *103* (19), 8577-8593.

31. Humphrey, W.; Dalke, A.; Schulten, K. VMD: visual molecular dynamics. *Journal of Molecular Graphics* **1996,** *14* (1), 33-38.

32. Izrailev, S.; Stepaniants, S.; Isralewitz, B.; Kosztin, D.; Lu, H.; Molnar, F.; Wriggers, W.; Schulten, K. Steered molecular dynamics. In *Computational molecular dynamics: challenges, methods, ideas*; Springer, **1999**, pp 39-65.

33. Ying, M.; Heng, Z.; Shiling, Y. Hydration Structure of Partially Hydrolyzed Preformed Particle Gel. *Chemiacal Journal of Chinese Universities-Chinese* **2015,** *36* (2), 386-394.

34. Liu, P.; Harder, E.; Berne, B. On the calculation of diffusion coefficients in confined fluids and interfaces with an application to the liquid-vapor interface of water. *The Journal of Physical Chemistry B* **2004,** *108* (21), 6595-6602.

35. Melnikov, S. M.; Höltzel, A.; Seidel-Morgenstern, A.; Tallarek, U. Composition, Structure, and Mobility of Water− Acetonitrile Mixtures in a Silica Nanopore Studied by Molecular Dynamics Simulations. *Analytical Chemistry* **2011,** *83* (7), 2569-2575.

36. Hower, J. C.; He, Y.; Bernards, M. T.; Jiang, S. Understanding the nonfouling mechanism of surfaces through molecular simulations of sugar-based self-assembled monolayers. *The Journal of Chemical Physics* **2006,** *125* (21), 214704.

37. Bandyopadhyay, S.; Chakraborty, S.; Bagchi, B. Secondary structure sensitivity of hydrogen bond lifetime dynamics in the protein hydration layer. *Journal of the American Chemical Society* **2005,** *127* (47), 16660-16667.

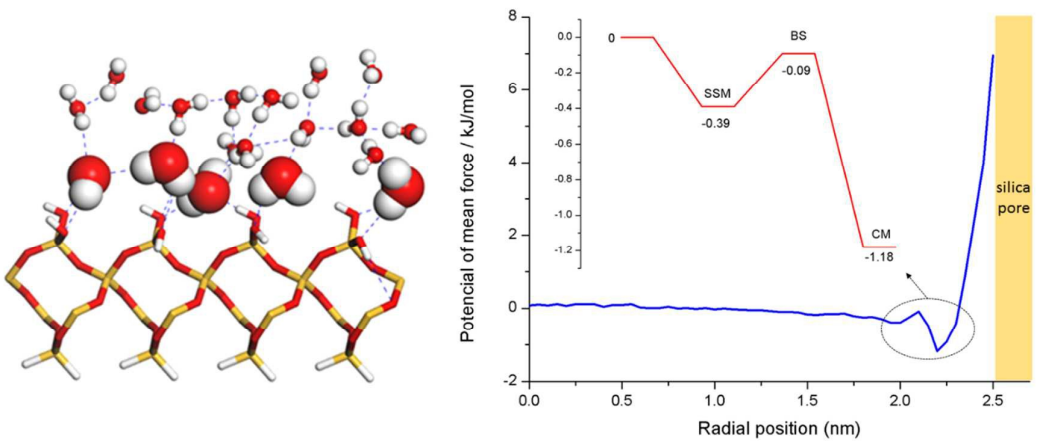

(a) (b)

TOC: Hydration layers induced by silanol groups at silica nanopore surface which served as a physical and energy barrier that keeps PPG away from the pore surface, and screened the interaction between PPG and pore. This largely reduced the resistance that PPG has to overcome during transport

(a) Water molecules within the first hydration layer were represented with CPK model, while in the second hydration layer were displayed in ball and stick model. Hydrogen bond network between them was illustrated as blue dashed lines. (b) Potential of mean force between water and silica nano pore